Intramolecular Proton Transfer in the Hydrogen Oxalate Anion and the Cooperativity Effects of the Low-Frequency Vibrations: A Driven Molecular Dynamics Study

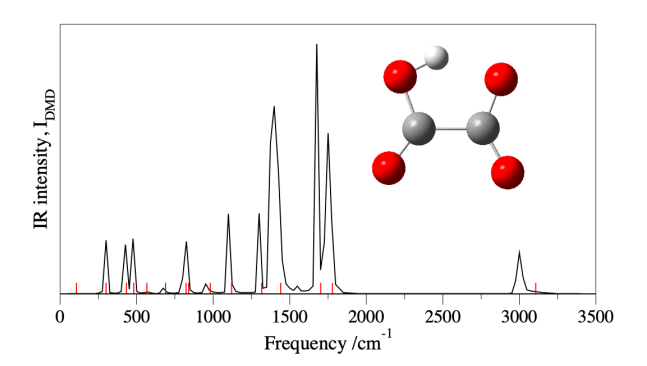
Dalton Boutwell, Dominick Pierre-Jacques, Olivia Cochran, Jason Dyke, Dayana Salazar, Ciara Tyler, Martina Kaledin*

Department of Chemistry & Biochemistry, Kennesaw State University, 370 Paulding Ave NW, Box # 1203, Kennesaw, GA 30144

ABSTRACT

We report first principles molecular dynamics (MD) and dipole driven molecular dynamics (μ-DMD) simulations of the hydrogen oxalate anion at the MP2/aug-cc-pVDZ level of theory. We examine the role of vibrational coupling between the OH stretching bands, i.e., the fundamental and a few combination bands spanning the 2900 - 3100 cm⁻¹ range, and several of the low-frequency bending and stretching fundamental modes. The low-frequency modes between 300 - 825 cm⁻¹ play a crucial role in the proton transfer motion. Strong involvement of CO₂ and CCO bending and the CC stretching vibrations indicate that these large amplitude motions cause the shortening of the O···O distance and thus promote H⁺ transfer to the other oxygen by bringing it over the 3.4 kcal/mol barrier. Analysis of resonant μ-DMD trajectories shows that the complex spectral feature near 825 cm⁻¹, closely corresponding to both an overtone of two quanta of 425 cm⁻¹ and a combination band of low-frequency CO₂ rocking (300 cm⁻¹) and CCO bending (575 cm⁻¹) modes is involved in proton transfer. μ-DMD shows that exciting the system at these mode combinations leads to faster barrier activation than exciting at the OH fundamental mode.

TOC Graphic



KEYWORDS Proton transfer, intramolecular proton transfer, hydrogen-bonding interaction, dipole driven molecular dynamics, normal mode analysis, combination bands, isotopic substitution, anharmonicity

I. INTRODUCTION

Proton transfer (PT) motion and hydrogen bonding interactions are used to describe some of the most fundamental processes in biology and chemistry. In this regard, PT is the central, primary component of the electron transport chain, acid-base chemistry, which includes the Grotthus mechanism and other reaction processes. Hydrogen oxalate, [C₂O₄H]⁻ is an anion derived from oxalic acid. The addition of a proton to the oxalate anion results in the cyclic geometry where the proton is located on the non-colinear path between two oxygen atoms. (As a side note, in the present paper, we prefer to use the terms 'colinear/non-colinear' for the O-H···O configuration to avoid confusion with the conventional terms 'linear/nonlinear' indicating a functional property or a dynamical process.) Hydrogen oxalate exhibits an asymmetric intramolecular hydrogen-bonded structure^{3,4} similar to molecular structures of malondialdehyde⁵ and acetylacetone⁶. In other intermolecular hydrogen bonded model systems, H₅O₂⁺ and H₃O₂⁻, the proton is located between the two oxygens along the colinear path: symmetrically in the middle of the O···O bond⁷ in H₅O₂⁺, while in the H₃O₂⁻, structure is very slightly asymmetric.⁸

On the other hand, hydrogen oxalate is a much more asymmetric hydrogen-bonded system with the proton bound between two oxygen atoms in a non-colinear configuration. The PT in oxalate occurs on the potential energy involving the barrier height 1200 cm⁻¹ (3.4 kcal/mol, CCSD(T)/aug-cc-pVTZ level of theory, see below) along the non-colinear O-H···O path. Therefore, it is expected that the spectral signatures of the PT motion will be significantly different for intramolecular vs. intermolecular hydrogen-bonded systems. Peluso et al. studied the effect of promoting low frequency bending vibrations on PT in 3-hydroxyflavone. Similarly, the ground state structure of 3-hydroxyflavone also exhibits a five-membered ring with an asymmetric intramolecular proton bond^{9,10} like the hydrogen bond in hydrogen oxalate. They found that large

amplitude CCO bending vibrations shorten the distance between the donor and acceptor oxygen atoms in the intramolecular hydrogen bonded structure that could favor the PT.⁹

The PT motion in [C₂O₄H]⁻ has been the subject of much experimental and theoretical work.^{3,4,11-13} Spectroscopic investigation of the PT process in [C₂O₄H]⁻ was first published by Truong et al., examining the rate constants of the PT and the probabilities of proton tunneling.¹¹ Using relationships between a proton, deuterium, and tritium oxalates, and based on standard calculations using the transition state theory (TST), Truong et al. concluded that tunneling effects are more important for deuterium than proton, especially at lower temperatures.¹¹ They found that at 300 K tunneling enhanced the transfer rate by 5% for proton and 40% for deuterium. Later on, Duan and Scheiner reported proton transfer rates and kinetic isotope effects (KIE) in a similar bent hydrogen bonded complex. Their findings on the effects of tunneling on KIE concluded that while the ZPE accounts for much of the KIE in deuterated complex, a considerable fraction of the KIE had occurred due to tunneling for the proton and deuteron.¹² Bosch et al. described the coupling of the O-H stretching and in-plane H bending modes to facilitate the PT as a non-colinear process.¹³

Hydrogen oxalate and its deuterated isotopologue have relatively low barrier heights for the proton/deuteron transfer process.^{3,4} Recent work points out that non-colinear PT in hydrogen oxalate anion is of interest due to its similarity with protonated glycine dipeptides.¹⁴ Several other studies of vibrational spectra of protonated peptides have uncovered diffuse spectral features in the vicinity of 2500 cm⁻¹ that correspond to pentagonal cyclic ionic hydrogen bond stretching modes. For instance, experimental predissociation spectra of [C₂O₄H]⁻.(H₂)₂ and [C₂O₄D]⁻.(H₂)₂ were reported by Wolke et al.³ covering mainly the higher frequency region of the spectra above 900 cm⁻¹. Hydrogen oxalate also exhibits such diffuse spectral features for the OH and OD-stretch vibrations that span over 2600-3400 cm⁻¹ and 1800-2200 cm⁻¹ range, respectively.^{3,4} In addition to

measuring the vibrational spectra, Wolke et al. made mode assignments using VPT2 and vibrational configuration interaction (VCI) calculations at the B3LYP/6-311++G(d,p) level of theory. However, the broad spectral feature in the OH/OD stretch regions was not retrieved at this level of theory, which led Wolke et al. to propose that this spectral feature originated in couplings between the high-frequency OH-stretch and the low-frequency COH bending along with deformation skeletal "doorway" vibrations.³

Theoretical studies by Xu and Meuwly⁴ used classical molecular dynamics (MD) and ring polymer MD simulations (RPMD) to obtain vibrational spectra of [C₂O₄H]⁻ and [C₂O₄D]⁻ that were directly compared to the available experiment.³ The quantum RPMD calculations produced broader IR spectra than the classical MD, although the effect of tunneling on the spectra was not discussed. The effective barrier height for the PT was modulated using a molecular mechanics proton transfer (MMPT) force field approach. Force field parameters were determined by fitting three different barrier heights (3.5, 4.2, and 4.5 kcal/mol) to *ab initio* calculations at the MP2/6-311++G(2d,2p) level of theory. Xu and Meuwly also reported MD simulations at B3LYP/6-31G levels of theory that produced satisfactory results compared to the experiment³ where it was concluded that a barrier height of 4.2 kcal/mol best reproduced the position and width of the IR absorption associated with the PT⁴.

In our previous work dealing with shared proton dynamics away from the harmonic limit, we analyzed vibrational spectra of protonated water clusters, ¹⁵⁻¹⁹ a protonated nitrogen dimer, N₄H⁺, ²⁰ and isoelectronic species N₂H⁺····OC, ²¹ using the dipole drive molecular dynamics method. Below, we refer to the dipole driven molecular dynamics method simply as DMD. We demonstrated that DMD can distinguish fundamentals, overtones, combination bands, and can identify anharmonic shifts. Importantly, DMD can be used to assign vibrational spectra in a wide

range of frequencies, including low-frequency parts in the far IR and terahertz regimes,²² which is particularly useful in the case of hydrogen oxalate.

The major aim of the present work is using DMD as a robust alternative to quantum vibrational methods to (i) describe the intramolecular PT motion in hydrogen oxalate and (ii) examine the cooperativity effects of the low frequency vibrations on PT activity. To reach this objective, we perform first principles molecular dynamics simulations to (a) generate IR spectra of hydrogen oxalate and its deuterium isotopologue and (b) assign prominent vibrational features, i.e., fundamentals, combination bands and overtones, by propagating and analyzing resonant DMD trajectories.

II. COMPUTATIONAL METHODS

Geometry optimization and frequency analysis for $[C_2O_4H]^-$ and $[C_2O_4D]^-$ global minimum and transition state for the PT were carried out at the MP2,²³⁻²⁵ CCSD,²⁶⁻²⁹ and CCSD(T)^{27,30,31} levels of theory with Dunning's basis sets^{32,33} aug-cc-pVDZ (AVDZ) and aug-cc-pVTZ (AVTZ).

To simulate the IR spectra, a total of 20 trajectories, with the initial conditions at the equilibrium geometry, were generated by sampling the velocities randomly from a uniform distribution and propagated for 10 ps as NVE ensemble with the total energy of 3128 cm⁻¹ (~300 K) using the velocity-Verlet integrator with a time step of 0.5 fs. The spectra were then obtained by a Fourier transform of the dipole-dipole correlation functions recorded along the trajectories and time-averaged over the length of the trajectories with a 4 ps signal window.²⁰

The DMD method allows trajectory analysis at each of the driving frequencies that absorb any amount of energy, thus making mode assignment possible. Our previously published works describe the details and recent implementation of the DMD method. 16,19,20 In DMD, an external,

sinusoidal electric filed is employed to cause an absorption at a resonant frequency, ω . The time-dependent Hamiltonian consists of the molecular Hamiltonian, H_0 , and a time-dependent driving term,

$$H(p,q,t;\omega) = H_0(p,q) + \vec{\mu}(q) \cdot \vec{\varepsilon} \sin \omega t \tag{1}$$

where $\vec{\mu}(q)$ is the coordinate-dependent electric dipole moment vector, and $\vec{\epsilon}$ is the electric field vector with the fixed laboratory frame Cartesian components X, Y, Z. The adapted equations of motion accounting for the driven term are

$$\dot{q} = \frac{p}{m} \tag{2a}$$

$$\dot{p} = -\nabla V(q) - (\nabla \vec{\mu}) \cdot \vec{\varepsilon} \sin \omega t \tag{2b}$$

where V(q) is the molecular interaction potential, m are atomic masses, and p and q are the 3N Cartesian momenta and coordinates, respectively. We typically vary the electric field strength on the [50,250] mV/bohr range to calibrate energy absorption. Present DMD simulations at fundamental frequencies were carried out with the electric field strength 130 mV/bohr. To induce appreciable energy absorption in combinations and overtone bands, that are forbidden in the double harmonic limit, we use the electric field at stronger intensity, 200 mV/bohr.

The DMD spectra were generated in the range of the experimentally known IR active vibrations³ between 50-2000 cm⁻¹ and 2600-3400 cm⁻¹ in the case of [C₂O₄H]⁻ with a frequency step of 25 cm⁻¹. Due to the H/D isotopic shift, the spectral range was 50-2400 cm⁻¹ in the case of [C₂O₄D]⁻. We run ~100 DMD trajectories for each isotopologue, [C₂O₄H]⁻and [C₂O₄D]⁻. Each DMD time step calculation requires 3 gradient evaluations, compared to just one gradient evaluation for each MD time step. Based on a broad comparison with several other methods (see below for more details), we have chosen MP2/AVDZ level of theory to evaluate the interaction

potential and dipole moment. The MD and DMD trajectories were propagated directly using MOLPRO 2019.1 program.³⁴

The average internal energy of the molecule is monitored along the driven trajectory, which is given by 19

$$I_{\rm DMD}(\omega) = \frac{1}{\tau} \int_0^{\tau} dt \, H(\mathbf{p}(t), \mathbf{q}(t); \omega). \tag{3}$$

It is expected to increase rapidly on resonance and oscillate off-resonance, whereby the resonant frequencies ω are identified. It is also a time-dependent quantity, and longer propagation times result in better spectral resolution.³⁵ At each resonant frequency, we examine the absorbed energy profiles, driving forces, dipole derivatives, atomic coordinates, calculate bond distances, bond angles, and dihedral angles to make the assignment of spectral features.

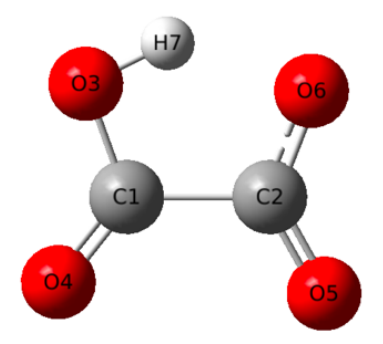


Figure 1. [C₂O₄H]⁻ global minimum configuration with atom labels, calculated with MP2/AVDZ. The molecule is oriented in the XY plane. The key interatomic distances are O3-H7=1.009 Å, O6-H7=1.677 Å, O3-O6=2.487 Å, bond angles O3-H7-O6=134.1 degrees, H7-O3-C1=97.7 degrees.

III. RESULTS AND DISCUSSION

III.A Hydrogen Oxalate structure and the Proton Transfer Barrier

Figure 1 shows the hydrogen oxalate, [C₂O₄H]⁻ global minimum geometry of the C_s symmetry. A comparison of the fully optimized structural parameters at various levels of theory are provided in the Supporting Information (**Tables S1 - S7**). At the global minimum, the O-H bond distance is very similar among all methods (within 0.01 Å); however, the O···H bond distance

varies significantly with the level of theory. The O-H and O···H bond distances are 1.000 Å and 1.687 Å, respectively at the CCSD(T)/AVTZ level of theory. For comparison, we evaluated the O-H and O···H distances in the asymmetric hydrogen-bonded complex, $H_3O_2^-$ (1.088 Å and 1.403 Å), and in the symmetric hydrogen bonded complex, $H_5O_2^+$ (1.195 Å and 1.195 Å) at the CCSD(T)/AVTZ level of theory. O···H bond distance in hydrogen oxalate is much longer compared to the one in $H_3O_2^-$.

Different structural parameters in the H₃O₂⁻, H₅O₂⁺, and [C₂O₄H]⁻ systems characterizing the hydrogen bond result in different intermolecular and intramolecular hydrogen bond energies. The presently computed zero-point corrected dissociation energies of the strongly bound interatomic hydrogen bonded systems H₃O₂⁻ and H₅O₂⁺ at the CCSD(T)/AVTZ level of theory are 26.2 and 33.3 kcal/mol, respectively. Very similar values were reported previously at the same levels of theory^{36,37} and the corresponding experimental values^{38,39} are 27.6 and 32.4 kcal/mol. The intramolecular hydrogen-bonded energy of the hydrogen oxalate cannot be simply estimated as the interaction energy, $E_{int}=E(AB)-[E(A)+E(B)]$. There are several methods to estimate the energy of intramolecular interactions. One of the frequently used methods is the so-called open-closed method, where the intramolecular interaction energy is evaluated as an energy difference between the open and closed (cyclic) forms.⁴⁰ The open form is generated by the rotation of the protondonor group. 40 We estimated the intramolecular hydrogen-bonded energy in hydrogen oxalate by simply rotating the C-C-O-H dihedral angle by 180 degrees without the full geometry optimization that would lead to the significant change in the structure.⁴⁰ The hydrogen oxalate energy of intramolecular interaction is thus estimated to be 12.4 kcal/mol at the CCSD(T)/AVTZ level of theory. The non-colinear hydrogen bond in the hydrogen oxalate is much weaker compared to a colinear hydrogen bond in H₃O₂⁻ and H₅O₂⁺. Intramolecular cyclic hydrogen-bonded structures

similar to hydrogen oxalate are malondialdehyde and acetylacetone. Their intramolecular interactions energies calculated at the MP2/6-31G** level of theory were 14.0 kcal/mol and 16.2 kcal/mol, respectively.⁴⁰ For comparison, the value for hydrogen oxalate is 13.6 kcal/mol calculated at the same level of theory, MP2/6-31G**.

Wolke et al. showed that the PT barrier height depends strongly on the level of electron correlation theory.³ They used B3LYP/6-311++G(d,p) calculations to assign the vibrational spectra and calculated a 3.4 kcal/mol barrier for PT at the B3LYP/6-311++G(d,p) level of theory. Xu and Meuwly reported a barrier height of 4.2 kcal/mol at the CCSD(T)/AVTZ level of theory.⁴ We also calculated the barrier height at the B3LYP, MP2, CCSD, and CCSD(T) levels of theory with multiple basis sets using fully optimized hydrogen oxalate minimum and transition state structures. The presently calculated CCSD(T)/AVTZ barrier height with full geometry optimization is 3.4 kcal/mol, noticeably different from the previously reported value of Xu and Meuwly.⁴ This difference is provisionally attributed to the latter's possible use of non-CCSD(T)/AVTZ optimized geometries for both structures. (See **Table S2** and **Table S6** in the Supporting Information). The CCSD(T)/AVTZ zero-point energy corrections reduce the barrier heights for the [C₂O₄H]⁻ and [C₂O₄D]⁻ to 1.1 and 1.8 kcal/mol, respectively. We note that the CCSD/AVTZ level of theory overestimates the barrier height and the MP2/AVTZ barrier height is smaller compared to the CCSD(T)/AVTZ value. The effect of the basis set size on the barrier height is rather different for B3LYP and for MP2, CCSD, CCSD(T) methods. Increasing the size of the basis set tends to increase the barrier height for B3LYP, while increasing basis size for MP2 and CC methods produces the opposite effect. The potential energy barrier heights and the corresponding ZPE corrected values at various levels of theory are summarized in **Table 1**.

III.B Vibrational mode analysis of [C₂O₄H]⁻ and [C₂O₄D]⁻

The harmonic frequencies and resonant peaks found in the MD and DMD spectra generated by the direct simulations at the MP2/AVDZ level of theory and those of the previous studies^{3,4} are shown in Table 2 and Table 3. Additional method comparisons can be found in the Supporting Information (Table S3, Table S4). Vibrational frequencies are distinguished as in-plane and outplane by the C_s symmetry labels, A' and A", respectively (see Figure S1, Figure S2 in the Supporting Information). Not surprisingly, the OH and OD stretch harmonic frequencies are more sensitive to the level of theory compared to bending and low deformation vibrations. The CCSD(T)/AVTZ harmonic frequencies for OH and OD stretch are 3202 and 2340 cm⁻¹, respectively. Carrying out direct trajectory simulations with MP2 or CCSD in conjunction with the AVTZ basis set is computationally too demanding for the seven-atom system with six heavy atoms. Careful examination of a large set of key properties reveals that the MP2/AVDZ level of theory yields sufficiently close agreement for structural parameters, barrier energy, dipole moments, and dipole derivatives with the corresponding CCSD(T)/AVTZ values. Based on this comparison, summarized in Table S1, we selected the MP2/AVDZ level of theory for MD and DMD simulations. In the following discussion, both the harmonic frequencies and the MD/DMDderived frequencies are assumed to be at this level of theory. Figure 2 shows the IR spectra for [C₂O₄H]⁻ and [C₂O₄D]⁻ calculated using the direct MD simulations.

Table 1. Potential energy barrier heights (in kcal/mol) and the corresponding ZPE corrected values for the proton and deuteron (values in parentheses) transfer processes calculated at various levels of theory.

Level of Theory	E _{TS} -E _{min}	ZPE-corrected
B3LYP/6-31+G(d,p)	2.8	0.6 (1.4)
B3LYP/6-311++G(d,p)	3.5	1.2 (2.0)
MP2/AVDZ	2.9	0.7 (1.4)
MP2/AVTZ	2.4	0.2 (0.9)
CCSD/AVDZ	4.7	2.3 (3.1)
CCSD/AVTZ	4.2	1.8 (2.6)
CCSD(T)/AVDZ	4.0	1.6 (2.4)
CCSD(T)/AVTZ	3.4	1.1 (1.8)

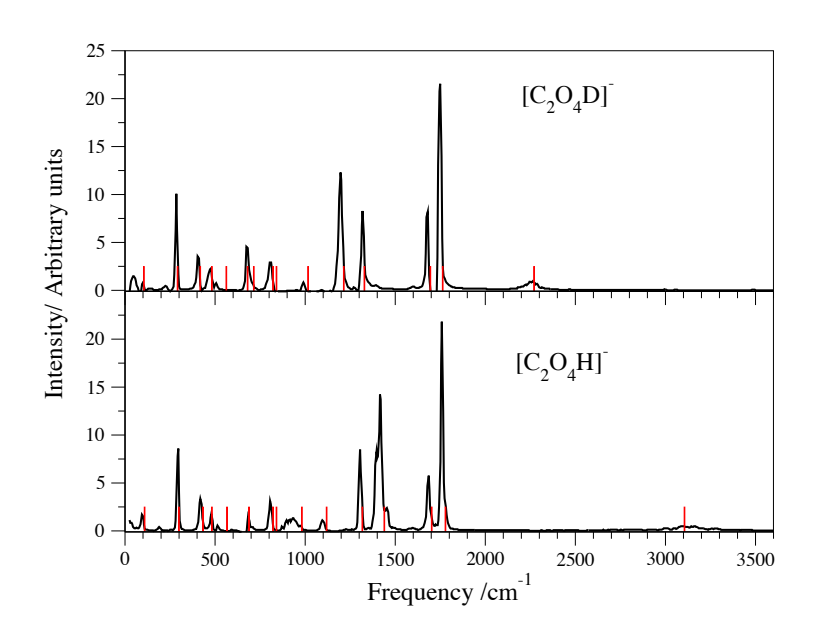


Figure 2. IR spectra of [C₂O₄H]⁻ and [C₂O₄D]⁻ calculated using the direct NVE MD MP2/AVDZ simulations propagated at total energy 3128 cm⁻¹ corresponding to 300 K temperature. 20 trajectories were propagated up to 10 ps with the time step 0.5 fs. The harmonic frequencies are shown as red sticks.

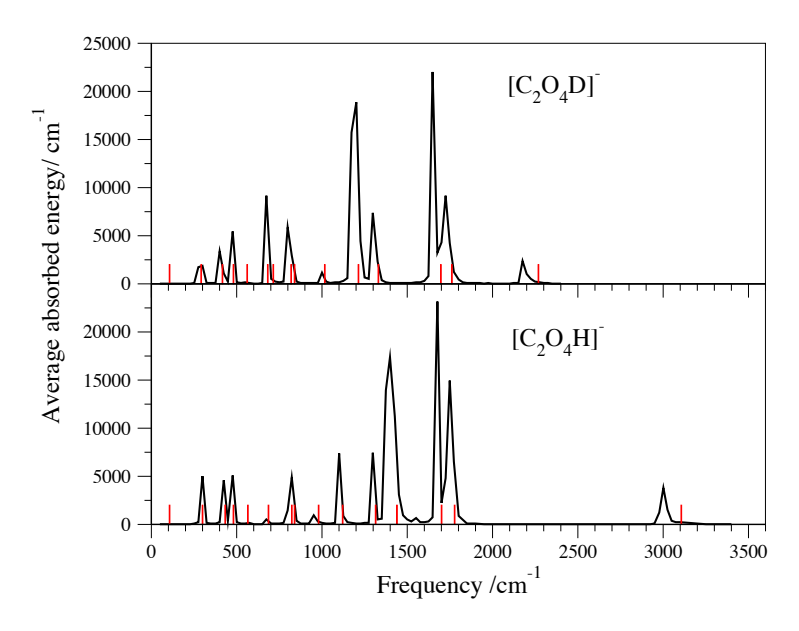


Figure 3. DMD MP2/AVDZ absorptions of $[C_2O_4H]^-$ and $[C_2O_4D]^-$ plotted as a function of driven frequency v_i . The DMD simulations were propagated up to 10 ps with the time step 0.5 fs. The intensity of the electric field was 130 mV/bohr. The harmonic frequencies are shown as red sticks.

Table 2. [C₂O₄H]⁻ Vibrational Frequencies (in cm⁻¹), C_s symmetry.

Frequency	NMA	MD-300 K	DMD	MMPT-V3 ⁴	MMPT-MD ⁴	Exp. ³
	MP2/AVDZ	MP2/AVDZ	MP2/AVDZ			
$\nu_1(A')$	3107	2800-3400	3000	2835	2860	2600-3400
$v_2(A')$	1779	1760	1750	1706	1765	1770-1820
$v_3(A')$	1703	1685	1675	1650	1715	1675-1700
$v_4(A')$	1441	1415	1400	1385	1410	1380-1430
$v_5(A')$	1317	1305	1300	1282	1335	1250-1330
$v_6(A')$	1120	1095	1100	1057	1095	1090
$v_7(A")$	981	930	950	929	920	940
$v_8(A")$	840	840	840	850	850	
ν ₉ (Α')	823	805	825	697	697	
$v_{10}(A')$	688	685	675	590	590	
$v_{11}(A')$	567	515	575	389		
$v_{12}(A")$	481	480	475	521		
$v_{13}(A')$	433	420	425	542		
ν ₁₄ (Α')	300	295	300	285		
$v_{15}(A")$	107	95	100	95		
$2v_{13}, v_{14}+v_{11}$	866	805	825			
$v_{11} + v_7$	1548	weak	1505			
$2v_4, v_5+v_2, nv_7+v_6$			3000			

Table 3. [C₂O₄D]⁻ Vibrational Frequencies (in cm⁻¹), C_s symmetry.

Frequency	NMA	MD-300 K	DMD	Exp. ³
	MP2/AVDZ	MP2/AVDZ	MP2/AVDZ	_
ν ₁ ' (Α')	2271	2265	2175	1800-2200
ν ₂ ' (Α')	1764	1750	1750	1780
ν ₃ ' (A')	1697	1680	1650	1600/1692/1728
ν ₄ ' (Α')	1214	1195	1200	1155/1217/1235
$v_5'(A')$	1330	1320	1300	1322/1339
ν_6 ' (A')	1015	990	1000	985
ν ₇ ' (Α")	714	675	675	
ν ₈ ' (A")	840	840	840	
ν ₉ ' (Α')	820	800	800	
$v_{10}'(A')$	682	675	675	
ν ₁₁ ' (A')	563	575	575	
ν ₁₂ ' (A'')	481	480	475	
ν ₁₃ ' (A')	417	405	400	
ν ₁₄ ' (Α')	294	285	300	
ν ₁₅ '(A'')	106	100	100	
v_{13} '+ v_2 ', v_7 '+ v_5 ', nv_{15} '+	$+v_2$ '		2175	

Vibrational predissociation spectra of $[C_2O_4H]^{-}$ - $(H_2)_2$ and $[C_2O_4D]^{-}$ - $(H_2)_2$ were measured and assigned by Wolke et al. using the extended Fermi approach.³ The OH stretch band was observed as a very broad and weak spectral feature in the range $2800 - 3400 \text{ cm}^{-1}$. The maximum peak in the OH stretch region was determined to be at 2945 cm^{-1} . In the same experiment, the OD-stretch spectral feature was less broad, $1800-2200 \text{ cm}^{-1}$ with the maximum occurring at 2100 cm^{-1} .³ The present MD simulations show a very weak and broad spectral feature near the OH stretching fundamental with multiple distinct maxima at 3000, 3100, and 3150 cm^{-1} . The corresponding OD stretching spectral region shows one distinct peak at 2265 cm^{-1} (Figure S3 in the Supporting Information). We then used these peak positions as guesses for DMD scans. The DMD spectra were generated in terms of averaged absorbed energy (Eq. 3) as a function of frequency (Figure 3). Importantly, the OH and OD stretch maximum peaks in the closely scanned DMD spectra were determined to be at 3000 cm^{-1} and 2175 cm^{-1} , respectively, in a good agreement with experiment³. The DMD spectra show a $\sim 100 \text{ cm}^{-1}$ anharmonic red shift for the OH/OD bands from their normal mode fundamentals (Figure 3).

Analysis of DMD trajectory driven at the OH-stretch frequency v_1 =3000 cm⁻¹ corresponding to the maximum in the DMD spectrum is shown in **Figure 4**. The trajectory does not begin to absorb energy up to ~5 ps while executing only small atomic displacements. After 5 ps, energy begins to be absorbed rapidly. Such a time delay followed by a rapid absorption is an important DMD signature that was observed in the driving of combination band frequencies of the N₄H⁺ cation,²⁰ and more recently in the driving of CH₄ at an overtone frequency.⁴¹ Thus, it is plausible to assume that the OH stretch near the fundamental frequency is mixed to some degree with the nearby overtone $2v_4$ at 2880 cm⁻¹ and various other combination bands. The first PT event occurs at approximately 5 ps in this DMD trajectory, shown as large R(H7-O3) atomic

displacements from 1.0 to 2.2 Å. Also, large R(O3-O6) atomic displacements and HOC, OCO, and CCO bond angle fluctuations indicate strong coupling of the OH-stretching and other stretching and bending vibrational modes. The broad spectral feature near 3000 cm⁻¹ as described by Wolke et al. using the VCI analysis³ was characterized as OH stretch "bright state" interacting with "doorway states" involving OH in-plane bending overtone and multiple combination bands of in-plane acid C-O stretching and C=O stretching, CO₂ asymmetric stretching and CO₂ symmetric stretching, in-plane OH bending and CO₂ asymmetric stretching. In addition to these combination bands, our DMD analysis revealed some large C-C stretching, OCO, and CCO bending angle displacements as well (Figure 4 and Figure S4). Also, later in the DMD trajectory (around 6 ps mark, see Figure S4 in the Supporting Information), the involvement of the out-ofplane vibrations is seen. (See also a movie in the Supporting Information). We speculate that the highly mixed OH stretch region near 3000 cm⁻¹ may include combination bands involving multiple quanta of low frequency modes $(n_iv_i + n_iv_i)$ in addition to those described by Wolke et. al.³ Further characterization of the broad spectral feature near the OH stretch region is the in-plane OH bending overtone $2v_4$, and combination bands of lower stretching and bending modes $v_5 + v_2$, $nv_7 + v_6$. The evidence for such assignment can be found in Figure S4. There are large C1-O3-H7 bond angle fluctuations related to the in-plane OH bending overtone $2v_4$ (Figure S4, panel B) The $v_5 + v_2$ combination band can be deduced from the large C-O stretching fluctuations (Figure 4). Some out-of-plane vibrations are involved due to large dihedral angle fluctuations (**Figure S4**, panel C). The pure OH stretching vibration is not geometrically favorable for a PT on a non-colinear path, unlike in the H₃O₂⁻ and H₅O₂⁺ systems. However, we propose that multiple combination bands and an overtone interact with the OH stretching mode that facilitates the PT.

Extensive DMD trajectory analysis provides further evidence of combination bands and overtones in the vibrational spectrum of $[C_2O_4H]^-$ at lower frequencies. The spectral feature near 825 cm⁻¹ (**Figure S5** in the Supporting Information) is ascribed to overlap of the fundamental mode, v_9 with either an overtone of two quanta of 425 cm⁻¹ ($2v_{13}$), or a combination band consisting of CO_2 rocking and CCO bending modes, $v_{14}+v_{11}$. There is another fundamental frequency, v_8 at 840 cm⁻¹ corresponding to the out-of-plane C=C bond motion in hydrogen oxalate that is dark (see IR intensities in the **Table S3**) and is therefore virtually non-absorbing in DMD. However, we propose that this dark mode v_8 is coupled to the IR active 823 cm⁻¹ v_9 mode both directly and possibly also via Fermi resonances with the $2v_{13}$ overtone and the $2v_{14}+v_{11}$ combination band that show up as out-of-plane motions in the 825 cm⁻¹ DMD trajectory (**Figure S5**, panel C).

We have also characterized a very weak, previously unreported spectral feature in the $[C_2O_4H]^-$ spectrum near 1505 cm⁻¹ (**Figure 3**). Based on the DMD analysis, this spectral feature is most likely a combination band of CCO bending and OH out-of-plane bending modes, $v_{11}+v_7$. Namely, **Figure S6** in the Supporting Information shows large C1-C2-O4 and C1-C2-O5 angle displacements and large displacements for H7-O3-C1-O4 dihedral angle. (See also a movie in the Supporting Information). For this calculation, the DMD trajectory was run with a stronger electric field of intensity 200 mV/bohr to induce sufficient energy absorption.

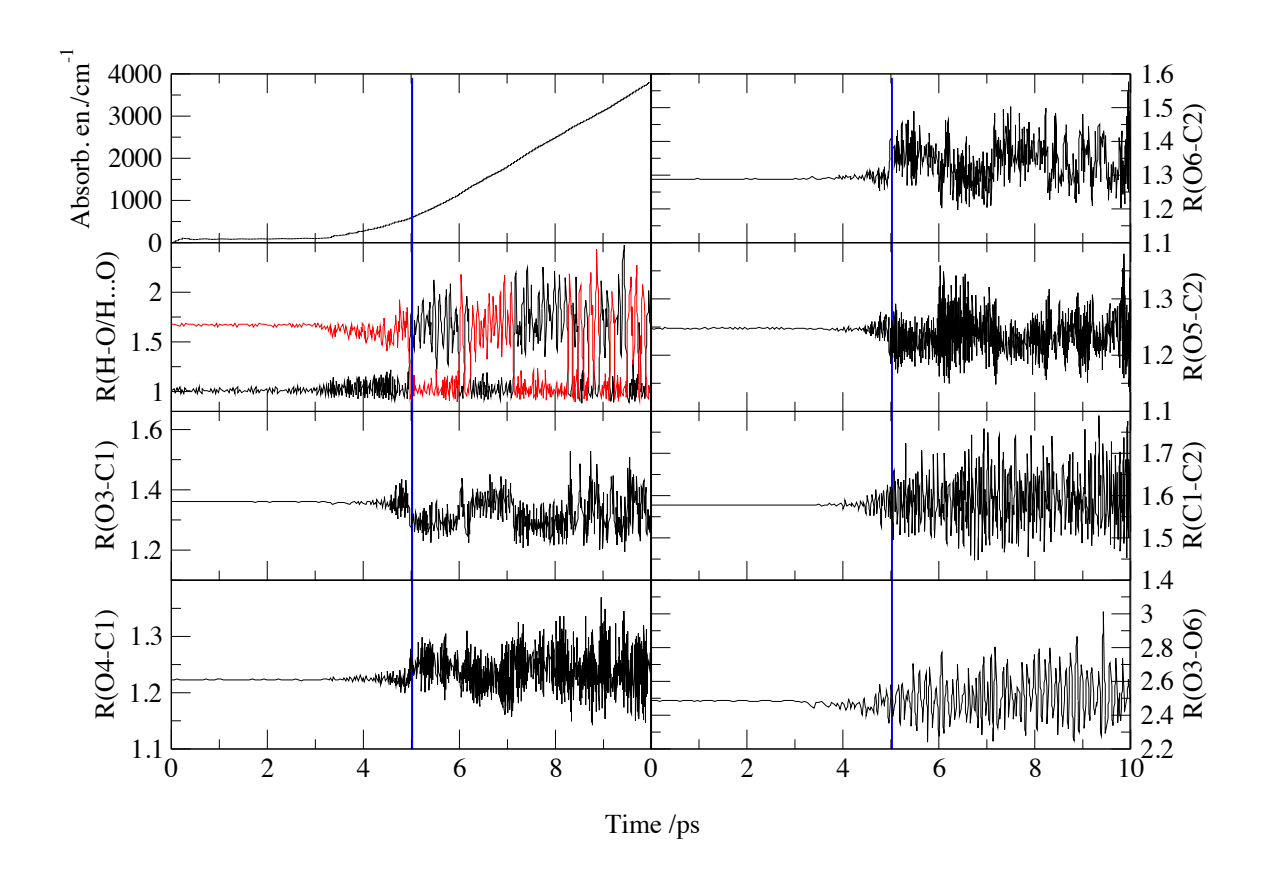


Figure 4. $[C_2O_4H]^-$ DMD trajectory driven at OH-stretching frequency v_1 =3000 cm⁻¹. Average absorbed energy is in cm⁻¹, interatomic distances are in Å. The H7-O3 distance is shown in black color, while H7...O6 distance in red color. The blue line indicates the proton transfer event. The intensity of the electric field was 130 mV/bohr. The atom labeling is shown in **Figure 1**.

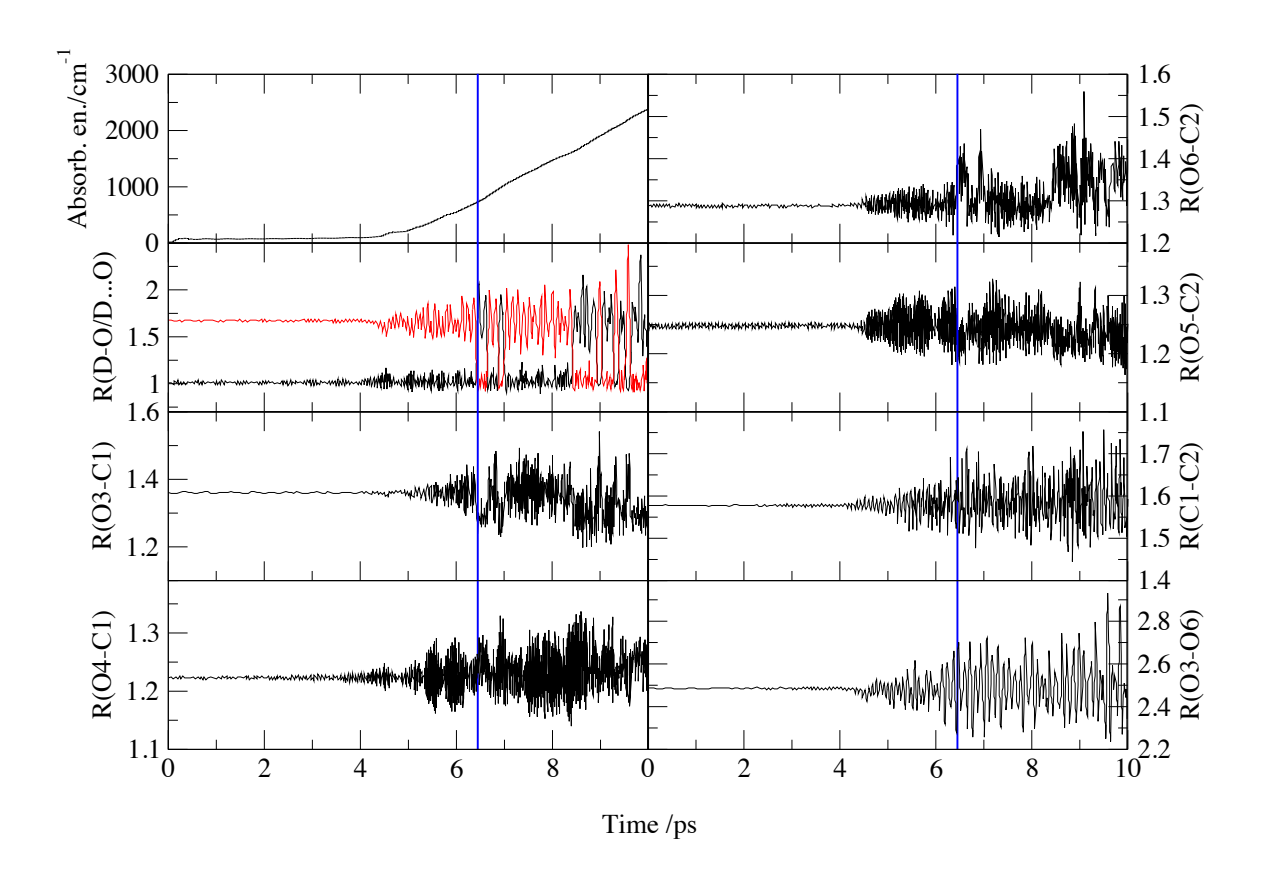


Figure 5. $[C_2O_4D]^-DMD$ trajectory driven at OD-stretching frequency $v_1'=2175$ cm⁻¹. Average absorbed energy is in cm⁻¹, interatomic distances are in Å. The D7-O3 distance is shown in black color, while D7...O6 distance in red color. The blue line indicates the proton transfer event. The intensity of the electric field was 130 mV/bohr.

Deuteration of the oxalate ion leads to a qualitatively different assignment for the OD-stretching region. Similar to the 3000 cm⁻¹ peak for OH, the broad spectral feature near 2200 cm⁻¹ was ascribed by Wolke et al.³ to the OD stretching "bright state" mixing with "doorway states" consisting of in-plane C=O acid stretching, OD out-plane bending, OD in-plane bending, and in-plane acid C-O stretching. Our DMD trajectory analysis (**Figure 5**) taken at the DMD peak maximum, v_1 '=2175 cm⁻¹ shows large atomic displacements for in-plane acid C=O stretching, OD in-plane bending modes, OD in-plane bending, and in-plane acid C-O stretching. Also, the C-C stretch, CCO, OCO bending, and O-C-C-O dihedral angles displacements are large, indicating the

involvement of other low-frequency modes as predicted by Wolke et al.³ The absorption energy profile shows a time delay up to 5 ps. The amount of energy absorbed at the OD-stretching frequency is much smaller compared to the OH-stretching frequency and the first PT event occurs later in $[C_2O_4D]^-$ (**Figure 5**) compared to $[C_2O_4H]^-$ (**Figure 4**). This is possibly due to the different vibrational coupling along the PT path, as well as the formal 1/m dependence of the absorbed energy on the oscillator mass at a resonance. 41 Deuteron transfer is clearly seen starting at ~6 ps when sufficient energy has been absorbed. However, based on an extended DMD trajectory analysis shown in Figure S7 and a simple sum of the fundamental harmonic frequencies seen in the **Table 3**, we propose an alternative assignment to the broad spectral feature at 2175 cm⁻¹ as the OD stretching mode appears strongly coupled with the bands involving multiple combinations, v_{13} '+ v_{2} ', v_{7} '+ v_{5} ', and nv_{15} '+ v_{2} '. The combination band v_{13} '+ v_{2} ' assignment arises from the substantial involvement of the CC stretching coordinate and an appreciable acid C=O stretching coordinate fluctuations seen commencing at 4 ps, well before the first PT event occurs (marked by the blue line at around 6.4 ps in Figure 5). The involvement of the out-of-plane C-O-D angle and D7-O3-C1-C2 dihedral angle fluctuations together with the C-O stretching coordinate fluctuations may be a sign of the v_7 ' + v_5 ' combination band. Also, extensive dihedral angle fluctuations for the C-C bond rotation imply contribution of the nv₁₅'+v₂'combination band.

III.C Dynamical Features of PT

The O-H···O configuration is not geometrically favorable for the proton to move directly to the other oxygen atom on a colinear path (**Figure 1**). As seen in the above discussion of the spectra, low-frequency deformation modes are expected to play a crucial role in facilitating the PT motion. In particular, the CO₂ bending, CCO bending, and CC stretching modes contribute to the substantial shortening of the O···O separation distance that can facilitate PT, bringing H/D over

the top of the barrier. To investigate the efficiency of the molecular vibration promoting PT, we compared times at which the first PT event occurred in [C₂O₄H]⁻ and [C₂O₄D]⁻. Note, the times at which PT occurs depend on the strength of the electric field and here we use the same field strength of 130 mV/bohr to compare involvement of vibrational mode in PT event. **Table 4** and movies in the Supporting Information show resonant frequencies at which the PT was seen. The DMD trajectories driven at low frequencies 300 cm⁻¹, 425 cm⁻¹, and 825 cm⁻¹ all resulted in PT motion that was activated significantly sooner, after ~1-3 ps, compared to the OH stretching mode at 3000 cm⁻¹ (**Figure 6**). We also note that PT is further delayed upon deuterium substitution for some modes (**Table 4**).

As a brief side note, we illustrate the key DMD mechanism by which the molecule absorbs energy from the electric field and, consequently, allows us to identify resonances. In the present simulations of IR activity, the electric field is coupled to the dipole moment, and thus an examination of the molecular dipole is pertinent. The driving forces were calculated as the negative first derivatives of the dipole moment projected onto the field vector, as seen in **Eq. 2b**, with respect to the Cartesian coordinates for each atom. **Figure 7** shows the driving forces acting on H atom for representative frequencies that involve PT motion. For a non-absorbing frequency used here as a calibrator of dipole activity (2600 cm⁻¹), the driving forces are virtually constant along the trajectory. The driving forces for the 3000 cm⁻¹ DMD trajectory, the OH fundamental frequency, show the largest oscillations for the H atom moving along the direction of PT (*X, Y* components). The weakly absorbing out-of-plane COH bending vibration at 950 cm⁻¹ shows rather small oscillations in the H⁺ driving force along the trajectory. The COH in-plane bending frequency at 1400 cm⁻¹ represents the strong IR spectral feature (**Figure 3**) and driving force oscillations are large, particularly at the early stages of the trajectory. In addition to the IR activity

inducing fast oscillations, one may also notice a slowly changing component in the driving force. That component is due to the rotation (re-alignment) of the molecule, a much slower process than vibration, in response to the coupling of the dipole moment with the field vector.

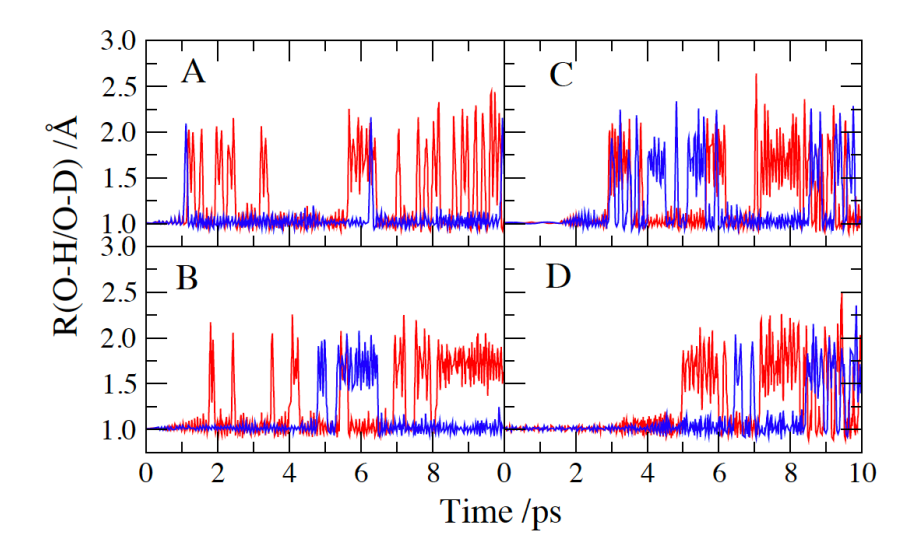


Figure 6. DMD trajectories analysis for visualization of the PT event in $[C_2O_4H]^-$ (in red) and $[C_2O_4D]^-$ (in blue). CO_2 in-plane rocking (v_{14}/v_{14}') CC stretching (v_{13}/v_{13}') , CO_2 symmetric bending (v_9/v_9') , and OH/OD stretching (v_1/v_1') vibrations are shown on panels A, B, C, D, respectively.

Table 4. Time of the first PT event seen in the DMD simulations propagated at the DMD identified resonant frequencies.

Freq	[C ₂ O ₄ H] ⁻	Time /ps	Freq	$[C_2O_4D]^-$	Time /ps
ν ₁ (Α')	3000	5.0	ν ₁ ' (A')	2175	6.4
$v_2(A')$	1750	3.6	ν ₂ ' (Α')	1750	8.5
$v_3(A')$	1675	1.1	ν ₃ ' (Α')	1650	2.6
ν ₄ (Α')	1400	1.4	ν ₄ ' (Α')	1200	1.1
ν ₅ (Α')	1300	6.4	ν ₅ ' (Α')	1300	7.1
$v_6(A')$	1100	1.4	ν ₆ ' (Α')	1000	-
ν ₇ (Α')	950	-	ν ₇ ' (Α')	675	7.7
ν ₉ (Α')	825	2.9	ν ₉ ' (Α')	800	3.0
$v_{13}(A')$	425	1.8	ν ₁₃ ' (Α')	400	4.8
ν ₁₄ (Α')	300	1.2	ν ₁₄ ' (Α')	300	1.1

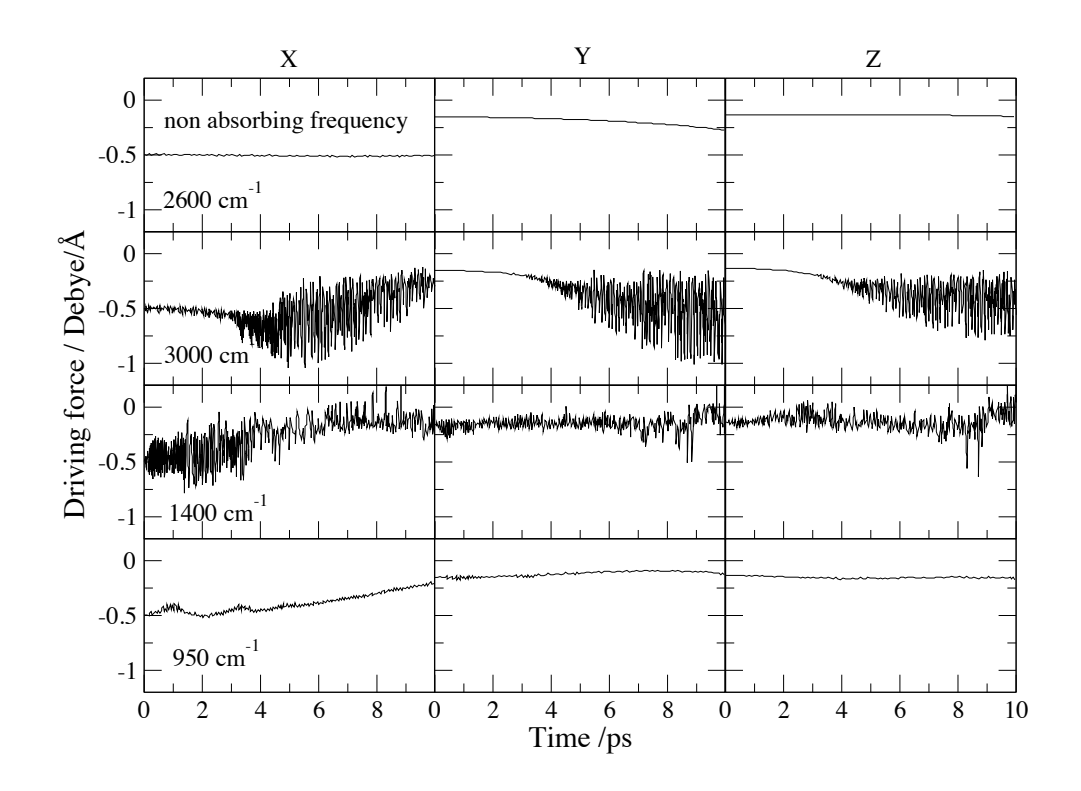


Figure 7. The driving force (Debye/Å) on the hydrogen atom along X, Y, (in plane) and Z (out of plane) for a non-absorbing frequency at 2600 cm⁻¹ and for active frequencies involving H⁺ motion: OH-stretching at 3000 cm⁻¹, COH in-plane bending at 1400 cm⁻¹, and out-of-plane COH bending at 950 cm⁻¹.

4. CONCLUSION

We have described first principles molecular dynamics and dipole driven molecular dynamics simulations of IR spectra of hydrogen oxalate anion at the MP2/aug-cc-pVDZ level of theory. In addition, we have examined the role of vibrational coupling between the OH stretching bands and several low-frequency bending and stretching fundamental modes. Analysis of the resonant electric field driven trajectories revealed several important findings:

- i) Lower frequency modes and combination bands, qualified as "doorway" states, cause proton transfer more efficiently compared to 3000 cm⁻¹ representing OH fundamental frequency as demonstrated by the analysis of the DMD trajectories propagated with same electric field strength of 130 mV/bohr. CO₂ bending, CCO bending, and CC stretching vibrations adjust O-H···O configuration favoring proton transfer at appreciably shorter times (after 1-3 ps of electric field exposure) compared to OH-stretching mode (after 5 ps of electric field exposure). In the [C₂O₄H]⁻ spectrum, a very weak, previously unreported spectral feature near 1505 cm⁻¹ was identified as a combination band of the CCO bending and OH out-of-plane bending modes; ii) Deuteration of the oxalate anion generally requires longer electric field exposure times to reach the H/D transfer transition state revealing a substantial KIE in this system, consistent with experiment.¹² However, as tunneling is expected to play a much greater role in the deuterated species,¹¹ the KIE is likely to be overestimated in the present classical DMD calculations;
- iii) The double harmonic approximation while giving a good representation of IR spectra and providing a useful reference picture for mode coupling, is not suitable for describing proton transfer in oxalate anion, and possibly other non-colinear shared proton systems;
- iv) Finally, we note that DMD is useful for assigning vibrational spectra over a wide range of frequencies, including the low-frequency regime as we demonstrated here. Given that DMD does not rely on a particular reference configuration (minimum, transition state, etc.) and can employ any coordinate system for making assignment, such as internal redundant coordinates, it can be used at least qualitatively, as a "measuring tool" of reaction rates involving large amplitude and floppy motions in shared hydrogen systems. Further calculations in this area are necessary to better establish this potentially highly valuable facility of DMD.

ASSOCIATED CONTENT

Supporting Information The Supporting Information is available free of charge on the ACS

Publications website. This contains structural parameters, harmonic vibrational frequencies,

overtones and combination bands, details of driven molecular dynamics analysis, and mpg

movies to visualize atomic motion.

AUTHOR INFORMATION

Corresponding Author

*Email: Martina Kaledin <u>mkaledin@kennesaw.edu</u>

ORCID

Martina Kaledin: 0000-0003-1763-3552

Dalton Boutwell: 0000-0002-6474-3394

Notes

The authors declare no competing financial interests.

ACKNOWLEDGEMENTS

This material is based upon work supported by the National Science Foundation under Grant No.

(CHE-1855583, DUE-1623723). Also, this work was supported in part by research computing

resources and technical expertise via a partnership between Kennesaw State University's Office

of the Vice President for Research and the Office of the CIO and Vice President for Information

Technology.⁴²

25

REFERENCES

- (1) Tymoczko, J.; Berg, J.; Stryer, L. Biochemistry A Short Course; W.H. Freeman and Company, New York, NY **2011**.
- (2) Grotthuss, C.J.T. Sur la décomposition de l'eau et des corps qu'elle tient en dissolution à l'aide de l'électricité galvanique, *Ann. Chim.* **1806**, *58*, 54-73.
- (3) Wolke, C. T.; DeBlase, A. F.; Leavitt, C. M.; McCoy, A. B.; Johnson, M. A. Diffuse Vibrational Signature of a Single Proton Embedded in the Oxalate Scaffold, HO₂CCO₂⁻. *J. Phys. Chem. A* **2015**, *119*, 13018-13024.
- (4) Xu, Z.-H.; Meuwly, M. Vibrational Spectroscopy and Proton Transfer Dynamics in Protonated Oxalate. *J. Phys. Chem. A* **2017**, *121*, 5389-5398.
- (5) Meuwly, M; Yang, Y. A Generalized Reactive Force Field for Nonlinear Hydrogen Bonds: Hydrogen Dynamics and Transfer in Malonaldehyde. *J. Chem. Phys.* **2010**, *133*, 064503.
- (6) Howard, D. L.; Kjaergaard, H. G.; Huang, J.; Meuwly, M. Infrared and Near-Infrared Spectroscopy of Acetylacetone and Hexafluoroacetylacetone. *J. Phys. Chem. A* **2015**, 119, 7980–7990.
- (7) McCoy, A.B.; Huang, X. C.; Carter, S.; Landerweer, M. Y.; Bowman, J. M. Full-dimensional Vibrational Calculations for H₅O₂⁺ Using an *ab initio* Potential Energy Surface. *J. Chem. Phys.* **2005**, *122*, 061101.
- (8) Diken, E. G.; Headrick, J.M.; Roscioli, J.R.; Bopp, J.C.; Johnson, M.A.; McCoy, A.B. Fundamental Excitations of the Shared Proton in the H₃O₂⁻ and H₅O₂⁺ Complexes. *J. Phys. Chem. A* **2005**, *109*, 1487-1490.
- (9) Peluso, A.; Adamo, C.; Del Re, G. A Theoretical Analysis of Excited State Proton Transfer in 3-hydroxyflavone Promoting Effect of a Low Frequency Bending Mode. *J. Math. Chem.* **1992**, *10*, 249-274.
- (10) Bellucci, M.; Coker, D.F. Molecular Dynamics of Excited State Intramolecular Proton Transfer: 3-hydroxyflavone in Solution. *J. Chem. Phys.* **2012**, *136*, 194505.

- (11) Truong, T. N.; McCammon, J. A. Direct Dynamics Study of Intramolecular Proton Transfer in Hydrogenoxalate Anion; *J. Am. Chem. Soc.* **1991**, *113*, 7504-7508.
- (12) Duan, X.; Scheiner, S. Energetics, Proton Transfer Rates, and Kinetic Isotope Effects in Bent Hydrogen Bonds, *J. Am. Chem. Soc.* **1992**, *114*, 5849-5856.
- (13) Bosch, E.; Miquel, M.; Lluch, J. M. The Role of Coupling in Intramolecular Proton Transfer Reactions. The Hydrogen Oxalate Anion as an Example; *Can. J. Chem.* **1992**, *70*, 100-106.
- (14) Leavitt, C. M.; DeBlase, A. F.; Johnson, C. J.; van Stipdonk, M.; McCoy, A. B.; Johnson, M. A. Hiding in Plain Sight: Unmasking the Diffuse Spectral Signatures of the Protonated N-Terminus in Isolated Dipeptides Cooled in Cryogenic Ion Trap. *J. Phys. Chem. Lett.* **2013**, *4*, 3450-3457.
- (15) Esser, T. K.; Knorke, H.; Asmis, K. R.; Schollkopf, W.; Yu, Q.; Qu, C.; Bowman, J. M.; Kaledin, M. Deconstructing Prominent Bands in the Terahertz Spectra of H₇O₃⁺ and H₉O₄⁺: Intermolecular modes in Eigen Clusters. *J. Phys. Chem. Lett.* **2018**, *9*, 798-803.
- (16) Kaledin, M.; Adedeji, D. T. Driven Molecular Dynamics Studies of the Shared Proton Motion in the H₅O₂⁺·Ar Cluster: The Effect of Argon Tagging and Deuteration on Vibrational Spectra; *J. Phys. Chem. A* **2015**, *119*, 1875-1884.
- (17) Kaledin, M.; Wood, C. A. Ab initio Studies of Structural and Vibrational Properties of Protonated Water Cluster H₇O₃⁺ and Its Deuterium Isotopologues: An Application of Driven Molecular Dynamics. *J. Chem. Theory Comput.* **2010**, *6*, 2525-2535.
- (18) Kaledin, M.; Kaledin, A. L.; Bowman, J. M.; Dong, J.; Jordan, K. D. Calculation of the Vibrational Spectra of H₅O₂⁺ and Its Deuterium-Substituted Isotopologues by Molecular Dynamics Simulations. *J. Phys. Chem. A* **2009**, *113*, 7671-7677.
- (19) Kaledin M.; Kaledin, A. L.; Bowman, J. M. Vibrational Analysis of the H₅O₂⁺ Infrared Spectrum Using Molecular and Driven Molecular Dynamics. *J. Phys. Chem. A* **2006**, *110*, 2933-2939.
- (20) Hooper, R.; Boutwell, D.; Kaledin, M. Assignment of Infrared-Active Combination Bands in the Vibrational spectra of Protonated Molecular Clusters Using Driven Classical Trajectories: Applications to N₄H⁺ and N₄D⁺. *J. Phys Chem. A* **2019**, *123*, 5613-5620.

- (21) Boutwell, D.; Okere, O.; Omodemi, O.; Toledo, A.; Barrios, A.; Olocha, M.; Kaledin, M. Analysis of the Proton Transfer Bands in the Infrared Spectra of Linear N₂H⁺···OC and N₂D⁺···OC Complexes Using Electric Field-Driven Classical Trajectories. *J. Phys. Chem. A* **2020**, *124*, 7549-7558.
- (22) Niehues, G.; Kaledin, A. L.; Bowman, J. M.; Havenith, M. Driving of a Small Solvated Peptide in the IR and THz Range A Comparative Study of Energy Flow. *J. Phys. Chem. B* **2012**, *116*, 10020–10025.
- (23) Head-Gordon, M.; Pople, J. A.; Frisch, M. J. MP2 Energy Evaluation by Direct Methods. *Chem. Phys. Lett.* **1988**, *153*, 503–506.
- (24) Sæbø, S.; Almlöf, J. Avoiding the Integral Storage Bottleneck in LCAO Calculations of Electron Correlation. *J. Chem. Phys. Lett.* **1989**, *154*, 83–89.
- (25) Frisch, M. J.; Head-Gordon, M.; Pople, J. A. A direct MP2 Gradient Method. *Chem. Phys. Lett.* **1990**, *166*, 275–280.
- (26) Čížek, J. in *Adv. in Chem. Phys.*, Ed. P. C. Hariharan, Vol. 14 (Wiley Interscience, New York, 1969) 35.
- (27) Purvis III, G. D.; and Bartlett, R. J. A Full Coupled-cluster Singles and Doubles Model the Inclusion of Disconnected Triples. *J. Chem. Phys.* **1982**, *76*, 1910-1918.
- (28) Scuseria, G. E.; Janssen, C. L.; Schaefer III, H. F. An Efficient Reformulation of the Closed-shell Coupled Cluster Single and Double Excitation (CCSD) Equations. *J. Chem. Phys.* **1988**, *89*, 7382-7387.
- (29) Scuseria G. E.; Schaefer III, H. F. Is Coupled Cluster Singles and Doubles (CCSD) More Computationally Intensive than Quadratic Configuration-interaction (QCISD)? *J. Chem. Phys.* **1989**, *90*, 3700-3703.
- (30) Gyevi-Nagy, L.; Kallay, M.; Nagy, P. R. Integral-Direct and Parallel Implementation of the CCSD(T) Method: Algorithmic Developments and Large-Scale Applications. *J. Chem. Theory Comput.* **2020**, *16*, 366-384.
- (31) Pople, J. A.; Head-Gordon, M.; Raghavachari, K. Quadratic Configuration Interaction a General Technique for Determining Electron Correlation Energies. *J. Chem. Phys.* **1987**, *87*, 5968-5975.

- (32) Dunning, T. H. Gaussian Basis Sets for Use in Correlated Molecular Calculations. I. The Atoms Boron Through Neon and Hydrogen. *J. Chem. Phys.* **1989**, *90*, 1007-1023.
- (33) Kendall, R. A.; Dunning, T. H.; Harrison, R. J. Electron Affinities of the First-row Atoms Revisited. Systematic Basis Sets and Wave Functions. *J. Chem. Phys.* **1992**, *96*, 6796-6806.
- (34) Werner, H.-J.; Knowles, P. J.; Knizia, G.; Manby, F. R.; Schütz, M.; Celani, P.; Györffy, W.; Kats, D.; Korona, T.; Lindh. R., et al. MOLPRO, version 2019.2, a package of ab initio programs, https://www.molpro.net.
- (35) Kaledin, M.; Kaledin, A. L.; Brown, A.; Bowman, J. M. In Normal-Mode Analysis: Theory and Applications to Biological and Chemical Systems; Q. Cui, I. Bahar, Eds.; CRC Press: Boca Raton, FL, (2005).
- (36) McCoy, A. B.; Huang, X.; Carter, S.; Bowman, J. M. Quantum Studies of the Vibrations in H₃O₂⁻ and D₃O₂⁻. *J. Chem. Phys.* **2005**, *123*, 064317.
- (37) Huang, X.; Braams, B. J.; Bowman, J. M. *Ab initio* potential energy and dipole moment surfaces for H₅O₂⁺. *J. Chem. Phys.* **2005**, *122*, 044308.
- (38) Kebarle, P.; Paul, G. J. C. Thermodynamics of the Association Reactions OH⁻ +H₂O= HOHOH⁻ and CH₃O⁻ + CH₃OH= CH₃OHOCH₃⁻ in the gas phase. *J. Phys. Chem.* **1990**, *94*, 5184-5189.
- (39) Dalleska, N. F.; Honma, K.; Armentrout, P. B. Stepwise Solvation of Protonated Water Clusters: Collision-Induced Dissociation as an Alternative to Equilibrium Studies. *J. Am. Chem. Soc.* **1993**, *115*, 12125-12131.
- (40) Jablonski, M. A Critical Overview of Current Theoretical Methods of Estimating the Energy of Intramolecular Interactions. *Molecules*, **2020**, *25*, 5512:1-37.
- (41) Pierre-Jacques, D.; Tyler, C.; Dyke, J.; Kaledin, A. L.; Kaledin, M. A polarizability driven ab initio molecular dynamics approach to stimulating Raman activity: Application to C₂₀. *Mol. Phys.* **2021**, *119*, e1939453:1-9.
- (42) Boyle T.; Ramazan, A. Kennesaw State University HPC Facilities and Resources. Digital Commons Training Materials, 10 (2021). https://digitalcommons.kennesaw.edu/training/10 (accessed December 10, 2021).

Supporting Information

Intramolecular Proton Transfer in the Hydrogen Oxalate Anion and the Cooperativity Effects of the Low-Frequency Vibrations: A Driven Molecular Dynamics Study

Dalton Boutwell, Dominick Pierre-Jacques, Olivia Cochran, Jason Dyke, Dayana Salazar, Ciara Tyler, Martina Kaledin*

Department of Chemistry & Biochemistry, Kennesaw State University, 370 Paulding Ave NW, Box # 1203, Kennesaw, GA 30144

This document contains the *XYZ* coordinates, structural parameters, dipole moments, dipole derivatives, and harmonic vibrational frequencies of [C₂O₄H]⁻ and [C₂O₄D]⁻ at the various levels of theory used in this work, MP2, CCSD(T) with aug-cc-pVDZ (AVDZ) and aug-cc-pVTZ (AVTZ) basis sets, and previous study B3LYP/6-311++G(d,p)¹ (**Tables S1 - S4**). Normal mode vectors of hydrogen (deuterium) oxalate anion and mode assignment are shown in **Figure S1** and **Figure S2**. We also report the *XYZ* coordinates, structural parameters, dipole moments, and harmonic vibrational frequencies of a transition state for the proton transfer (**Tables S5 - S7**). The main text shows the IR spectra and DMD spectra of [C₂O₄H]⁻ and [C₂O₄D]⁻ in the full range. Here we display the OH/OD stretching region (**Figure S3**). DMD trajectories are visualized as time dependence of interatomic distances, bond angles, and dihedral angles collected along the trajectory (**Figures S4 - S7**). Also, we generated movies by the VMD software² using the coordinates obtained from the DMD trajectories driven at frequencies 300, 425, 825, 1505, and 3000 cm⁻¹ for hydrogen oxalate anion and DMD trajectories driven at frequency 2175 cm⁻¹ for its deuterium analogue.

Corresponding Author

*Email: Martina Kaledin, mkaledin@kennesaw.edu

Table S1. $[C_2O_4H]^-$ interatomic distances (in Å), dipole moments, $^a\mu$ (in atomic units), and dipole derivatives for hydrogen atom only (atomic units). The atom labeling of the global minimum (C_s symmetry) is shown in the main text, **Figure 1**.

Method/ Basis set	B3LYP/ 6311++G(d,p)	MP2/ AVDZ	MP2/ AVTZ	CCSD(T)/ AVDZ	CCSD(T)/ AVTZ
C1-C2	1.594	1.578	1.574	1.586	1.581
C1-O3	1.351	1.361	1.348	1.365	1.350
C1-O4	1.206	1.223	1.213	1.221	1.210
C2-O5	1.230	1.248	1.236	1.246	1.235
C2-O6	1.270	1.288	1.277	1.285	1.274
О3-Н7	1.000	1.009	1.009	1.002	1.000
О6-Н7	1.713	1.677	1.647	1.739	1.687
C1-C2-O5	118.4	118.7	118.8	118.4	118.4
C1-C2-O6	110.6	110.8	110.5	110.8	110.7
C1-O3-H7	99.7	97.7	97.4	98.7	98.5
C2-C1-O3	109.4	109.4	109.1	109.7	109.4
C2-C1-O4	127.8	127.8	127.7	127.8	127.7
C2-O6-H7	88.9	88.0	88.2	88.2	88.3
O3-H7-O6	131.5	134.1	134.8	132.6	133.1
μ_{x}	0.7120	0.6582	0.6572	0.6653	0.6700
μ_{y}	0.7279	0.7089	0.6803	0.7448	0.7205
μ_z	0.0000	0.0000	0.0000	0.0000	0.0000
μ	1.0182	0.9673	0.9458	0.9987	0.9839
dμ _x /dx _H	0.4781	0.4956	0.5114	0.4615	0.4580
dμ _x /dy _H	0.1529	0.1527	0.1498	0.1591	0.1609
dμ _x /dz _H	0.1616	0.1340	0.1328	0.1365	0.1374

^aThe center of mass molecular orientation was used to calculate the dipole moments.

Table S2. XYZ coordinates (Å) for the hydrogen oxalate $[C_2O_4H]^-$ global minimum structure, $(C_s \text{ symmetry})$ optimized with CCSD(T)/AVTZ. The minimum energy is -377.320032 Hartree, and the corresponding zero-point corrected values is -377.283766 Hartree.

Atom	X	Y	Z
C	0.7142833363	-0.2422174428	0.0000000000
\mathbf{C}	-0.8663237638	-0.2225765718	0.0000000000
O	1.1785385887	1.0258883026	0.0000000000
O	1.4416486828	-1.2094033883	0.0000000000
O	-1.4672304566	-1.3009910623	0.0000000000
O	-1.3011647637	0.9747545528	0.0000000000
Н	0.3002483763	1.5045446097	0.0000000000

Table S3. [C₂O₄H]⁻ harmonic vibrational frequencies (in cm⁻¹), IR intensities in parentheses (in km/mol).

Method/	B3LYP/	MP2/	MP2/	CCSD(T)/	CCSD(T)/
Basis set	6-311++G(d,p)	AVDZ	AVTZ	AVDZ	AVTZ
ω ₁ (A')	3201 (400)	3107 (417)	3067 (451)	3221 (362)	3202 (392)
ω ₂ (A')	1816 (503)	1779 (466)	1799 (511)	1792 (416)	1817 (456)
ω ₃ (A')	1731 (318)	1703 (207)	1727 (197)	1696 (264)	1727 (263)
ω ₄ (A')	1441 (586)	1441 (603)	1449 (617)	1447 (588)	1456 (594)
ω ₅ (A')	1318 (176)	1317 (151)	1329 (153)	1318 (168)	1335 (169)
ω ₆ (A')	1117 (49)	1120 (33)	1135 (25)	1120 (40)	1140 (32)
ω ₇ (A")	935 (85)	981 (60)	1005 (59)	947 (62)	969 (62)
ω ₈ (A")	837 (0.08)	840 (0.01)	851 (0.01)	836 (0.02)	849 (0.1)
ω ₉ (A')	820 (53)	823 (41)	830 (41)	819 (42)	829 (43)
ω ₁₀ (A')	704 (25)	688 (25)	700 (24)	687 (27)	701 (26)
ω ₁₁ (A')	563 (3)	567 (2)	572 (3)	558 (3)	566 (3)
ω ₁₂ (A")	482 (40)	481(31)	488 (30)	481 (34)	489 (34)
ω ₁₃ (A')	419 (16)	433 (24)	434 (27)	432 (19)	435 (21)
ω ₁₄ (A')	296 (19)	300 (19)	299 (21)	301 (17)	301 (18)
ω ₁₅ (A")	102 (0.6)	107 (0.4)	110 (0.4)	102 (0.5)	104 (0.5)

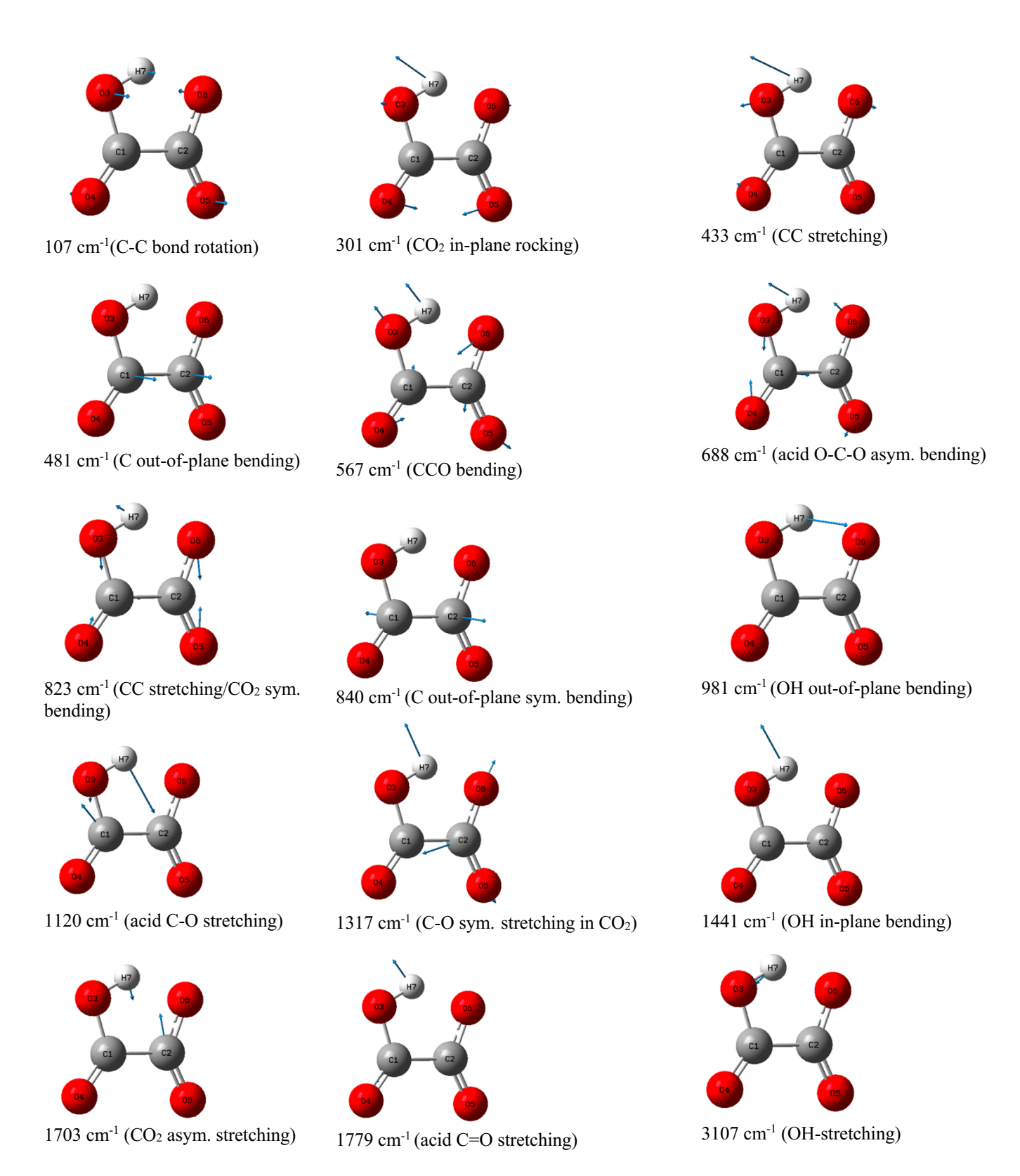


Figure S1. MP2/AVDZ normal mode vectors of hydrogen oxalate and the mode assignment visualized by the Gaussview program.

Table S4. [C₂O₄D]⁻ harmonic vibrational frequencies (in cm⁻¹), IR intensities in parentheses (in km/mol).

Method/	B3LYP	MP2	MP2	CCSD(T)	CCSD(T)
Basis set	6-311++G(d,p)	AVDZ	AVTZ	AVDZ	AVTZ
ω ₁ (A')	2339 (211)	2271 (219)	2243 (232)	2352 (194)	2340 (207)
ω ₂ (A')	1804 (517)	1764 (490)	1785 (537)	1776 (433)	1802 (473)
ω ₃ (A')	1726 (441)	1697 (329)	1719 (320)	1690 (393)	1721 (388)
ω ₄ (A')	1220 (333)	1214 (277)	1233 (273)	1213 (282)	1236 (281)
ω ₅ (A')	1324 (200)	1330 (206)	1340 (203)	1330 (227)	1347 (221)
ω ₆ (A')	1014 (9)	1015 (17)	1022 (22)	1018 (11)	1026 (16)
ω ₇ (A")	695 (23)	714 (35)	731 (35)	690 (38)	706 (38)
ω ₈ (A")	837 (0)	840 (0.2)	851 (0.2)	836 (0.05)	850 (0.09)
ω ₉ (A')	817 (60)	820 (46)	827 (48)	816 (47)	826 (48)
ω ₁₀ (A')	682 (50)	682 (24)	693 (22)	680 (25)	693 (24)
ω ₁₁ (A')	558 (3)	563 (2)	568 (2)	554 (3)	561 (3)
ω ₁₂ (A")	482 (37)	481 (29)	486 (29)	480 (32)	488 (31)
ω ₁₃ (A')	404 (14)	417 (21)	418 (24)	417 (17)	419 (19)
ω ₁₄ ' (A')	289 (22)	294 (22)	292 (25)	295 (19)	294 (21)
ω ₁₅ (A")	102 (0.6)	106 (0.4)	109 (0.4)	101 (0.5)	103 (0.5)

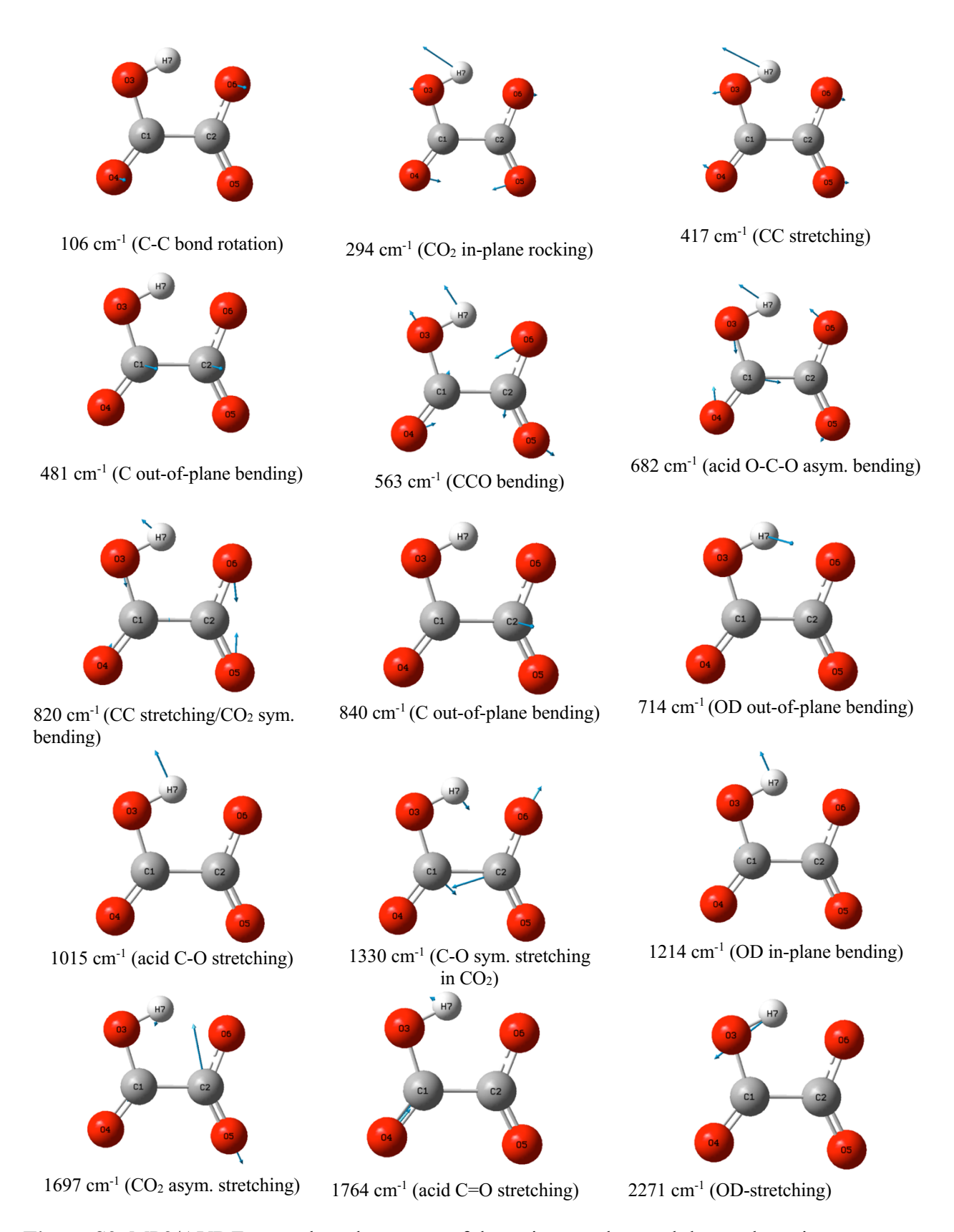


Figure S2. MP2/AVDZ normal mode vectors of deuterium oxalate and the mode assignment visualized by the Gaussview program.

Table S5. $[C_2O_4H]^-$ transition state interatomic distances (in Å) (C_{2v} symmetry), dipole moments^a, μ (atomic units). The atom labeling is shown in the main text, **Figure 1**.

Method/ Basis set	B3LYP/ 6-311++G(d,p)	MP2/ AVDZ	MP2/ AVTZ	CCSD(T)/ AVDZ	CCSD(T)/ AVTZ
C1-C2	1.593	1.578	1.575	1.586	1.581
C1-O3	1.306	1.322	1.310	1.322	1.309
C1-O4	1.217	1.234	1.223	1.232	1.221
C2-O5	1.217	1.234	1.223	1.232	1.221
C2-O6	1.306	1.322	1.310	1.322	1.309
О3-Н7	1.225	1.230	1.222	1.229	1.221
O6-H7	1.225	1.230	1.222	1.229	1.221
C1-C2-O5	125.1	125.0	124.9	125.0	125.0
C1-C2-O6	106.3	106.9	106.8	106.6	106.6
C1-O3-H7	92.0	90.8	90.8	91.1	91.2
C2-C1-O3	106.3	106.9	106.8	106.6	106.6
C2-C1-O4	125.1	125.0	124.9	125.0	125.0
C2-O6-H7	92.0	9190.8	90.8	91.1	91.2
O3-H7-O6	143.4	144.7	144.9	144.5	144.6
μ	0.6013	0.5604	0.5655	0.5564	0.5655

^aThe center of mass molecular orientation was used to calculate the dipole moments.

Table S6. XYZ coordinates (Å) for the hydrogen oxalate $[C_2O_4H]^-$ transition state geometry $(C_{2v}$ symmetry) optimized with CCSD(T)/AVTZ. The energy is -377.314691 Hartree, and the corresponding zero-point corrected values is -377.282075 Hartree.

Atom	X	Y	Z
C	0.7516265673	-0.2184981571	0.0000000000
C	-0.8294068820	-0.2402467807	0.0000000000
O	1.1065757928	1.0418390152	0.0000000000
O	1.4649187290	-1.2093774221	0.0000000000
O	-1.5151736394	-1.2503685317	0.0000000000
O	-1.2188859328	1.0098514363	0.0000000000
Н	-0.0612546350	1.3968004400	0.0000000000

Table S7. harmonic vibrational frequencies (in cm $^{-1}$) of $[C_2O_4H]^-$ transition state (C_{2v} symmetry).

Method/	B3LYP/	MP2/	MP2/	CCSD(T)/	CCSD(T)/
Basis set	6-311++G(d,p)	AVDZ	AVTZ	AVDZ	AVTZ
$\omega_1(B_2)$	-1115	-1087	-994	-1226	-1143
$\omega_2(A_2)$	143	142	143	140	142
$\omega_3(A_1)$	329	334	335	333	334
$\omega_4(B_1)$	488	486	492	485	493
$\omega_5(B_2)$	605	602	606	596	603
$\omega_6(A_1)$	702	701	711	703	715
ω ₇ (B ₂)	757	738	754	733	751
$\omega_8(A_2)$	839	843	853	840	853
ω ₉ (A ₁)	862	853	864	851	866
$\omega_{10}\left(\mathrm{B}_{2}\right)$	1262	1273	1291	1266	1298
$\omega_{11}(B_1)$	1297	1280	1302	1284	1300
$\omega_{12}(A_1)$	1299	1310	1321	1305	1323
$\omega_{13}(A_1)$	1745	1715	1739	1719	1749
$\omega_{14}(B_2)$	1797	1757	1783	1759	1791
$\omega_{15}(A_1)$	2076	2057	2081	2074	2101

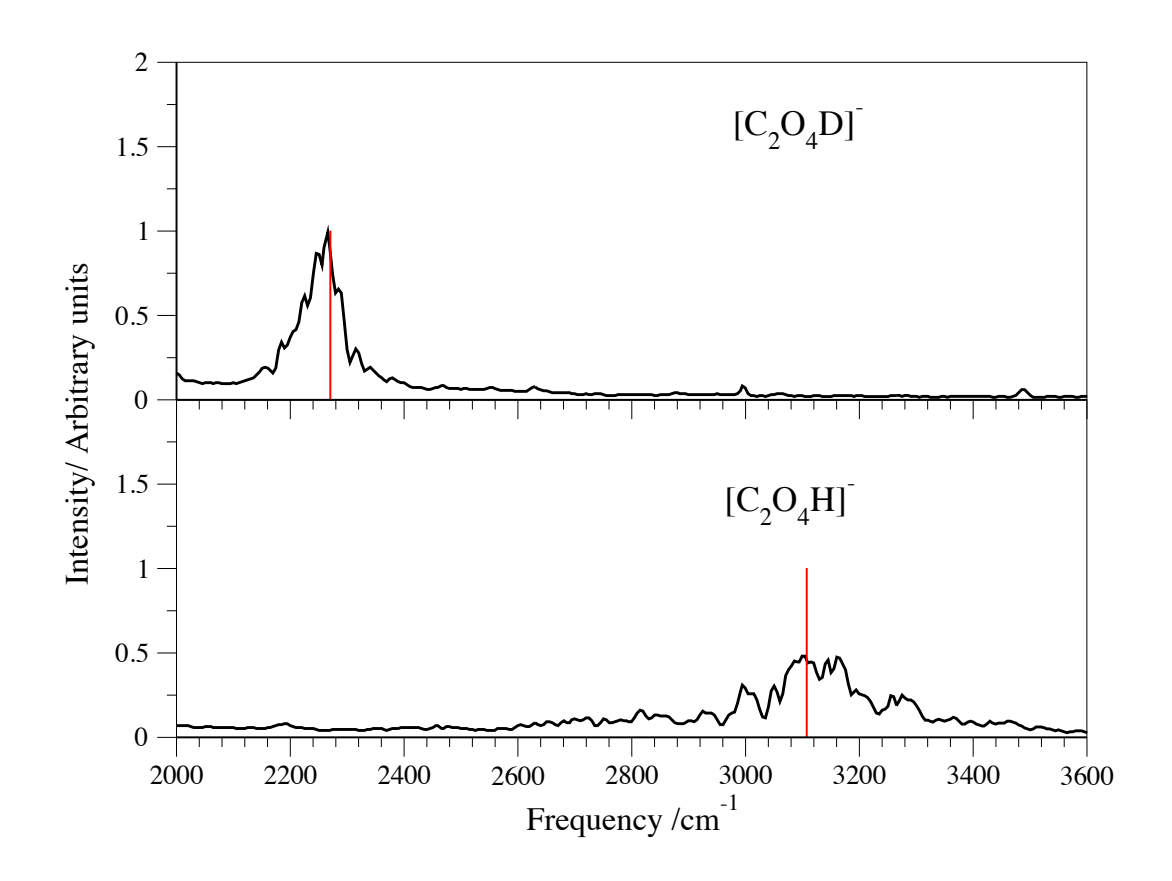


Figure S3. Infrared spectra of [C₂O₄H]⁻ and [C₂O₄D]⁻ in the OH/OD stretching region obtained from direct MD-MP2/AVDZ simulations at 300 K. The harmonic frequencies are shown as red sticks. The full range MD spectrum can be found in the main text, **Figure 2**.

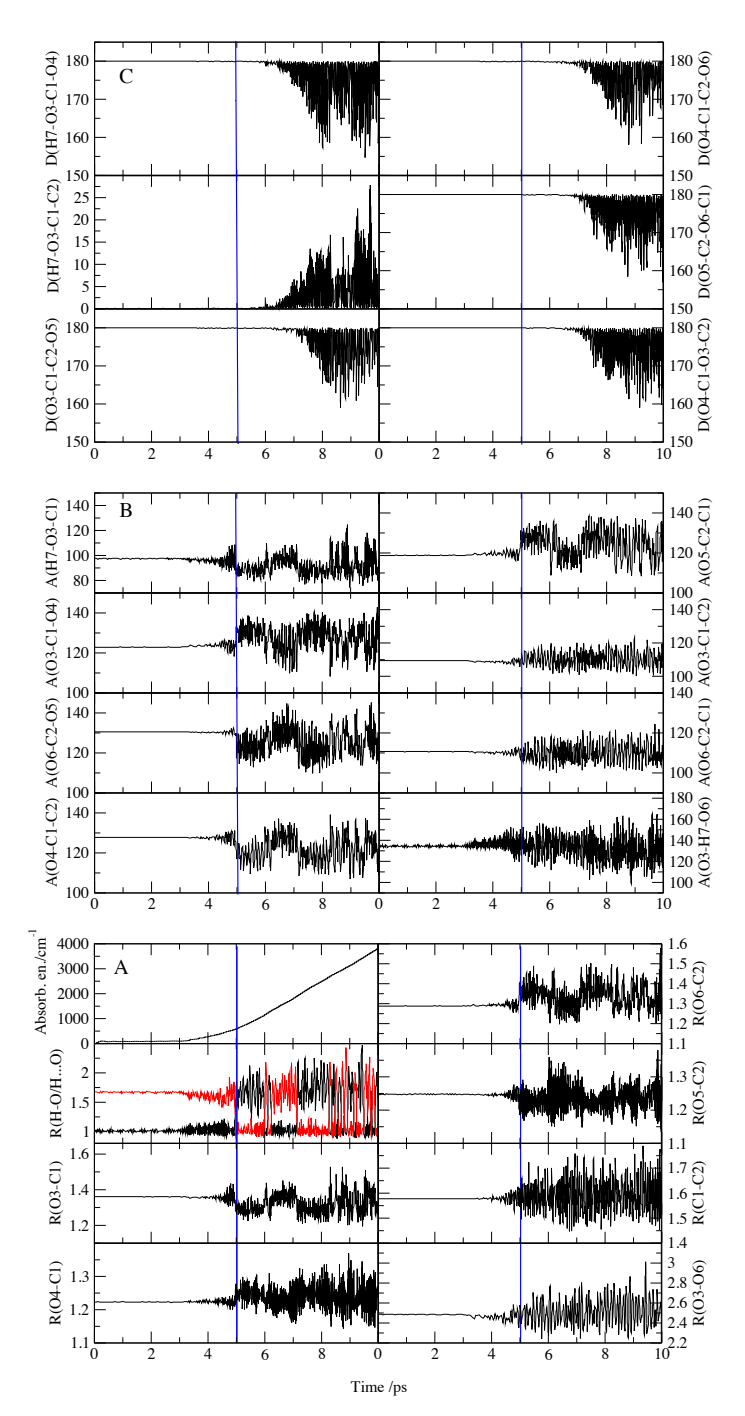


Figure S4. $[C_2O_4H]^-$ DMD trajectory driven at OH-stretching frequency v_1 =3000 cm⁻¹. Average absorbed energy is in cm⁻¹, interatomic distances are in Å (bottom panel, A). The H7-O3 distance is shown in black color, while H7...O6 distance in red color. Bond angles (middle panel, B), and dihedral angles (top panel, C) are in degrees. The blue line indicates the first proton transfer event. The intensity of the electric field was 130 mV/bohr. The atom labeling is shown in the main text, **Figure 1**.

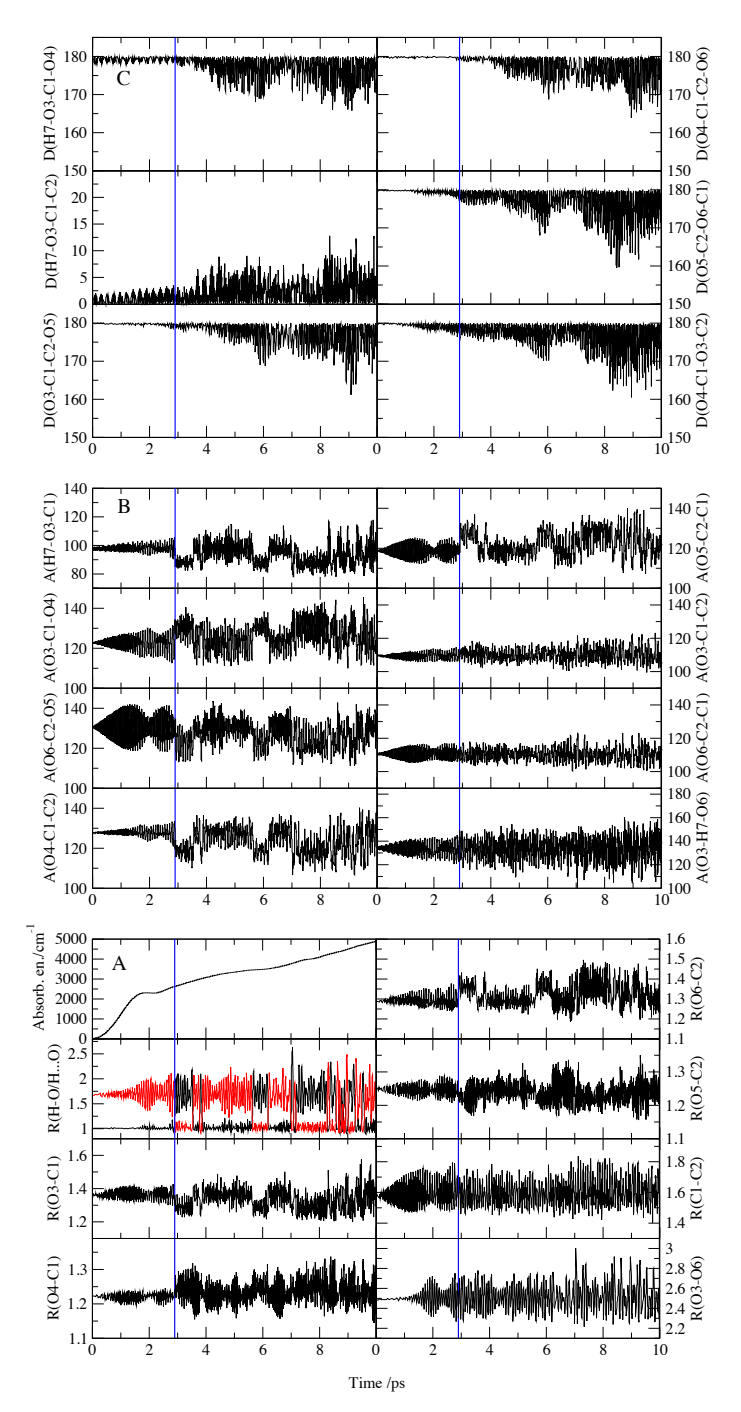


Figure S5. $[C_2O_4H]^-$ DMD trajectory driven at CC stretching/CO₂ symmetric bending fundamental frequency, v_9 =825 cm⁻¹. Average absorbed energy is in cm⁻¹, interatomic distances are in Å (bottom panel, A). The H7-O3 distance is shown in black color, while H7...O6 distance in red color. Bond angles (middle panel, B), and dihedral angles (top panel, C) are in degrees. The intensity of the electric field was 130 mV/bohr.

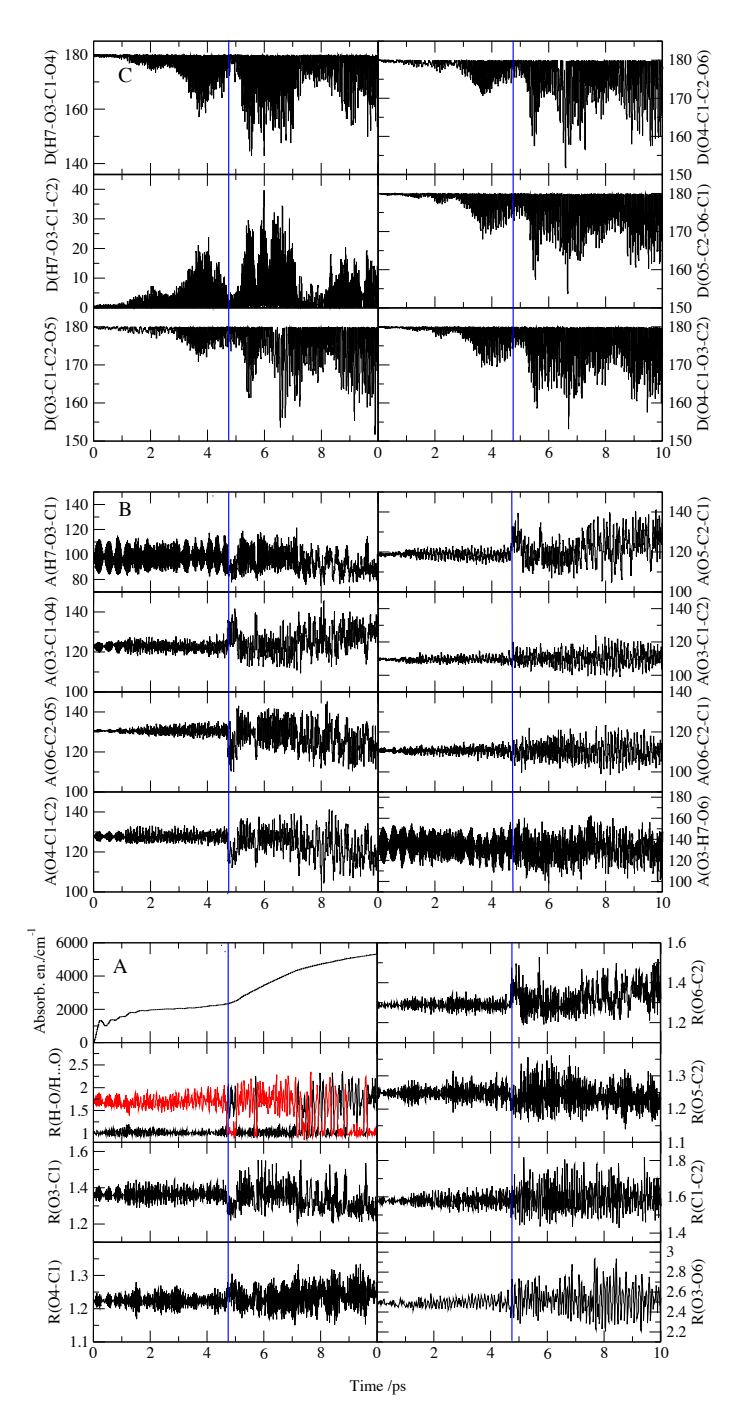


Figure S6. [C₂O₄H]⁻ DMD trajectory driven at combination band $v_{11}+v_7=1505$ cm⁻¹. Average absorbed energy is in cm⁻¹, interatomic distances are in Å (bottom panel, A). The H7-O3 distance is shown in black color, while H7...O6 distance in red color. Bond angles (middle panel, B), and dihedral angles (top panel, C) are in degrees. The intensity of the electric field was stronger, 200 mV/bohr.

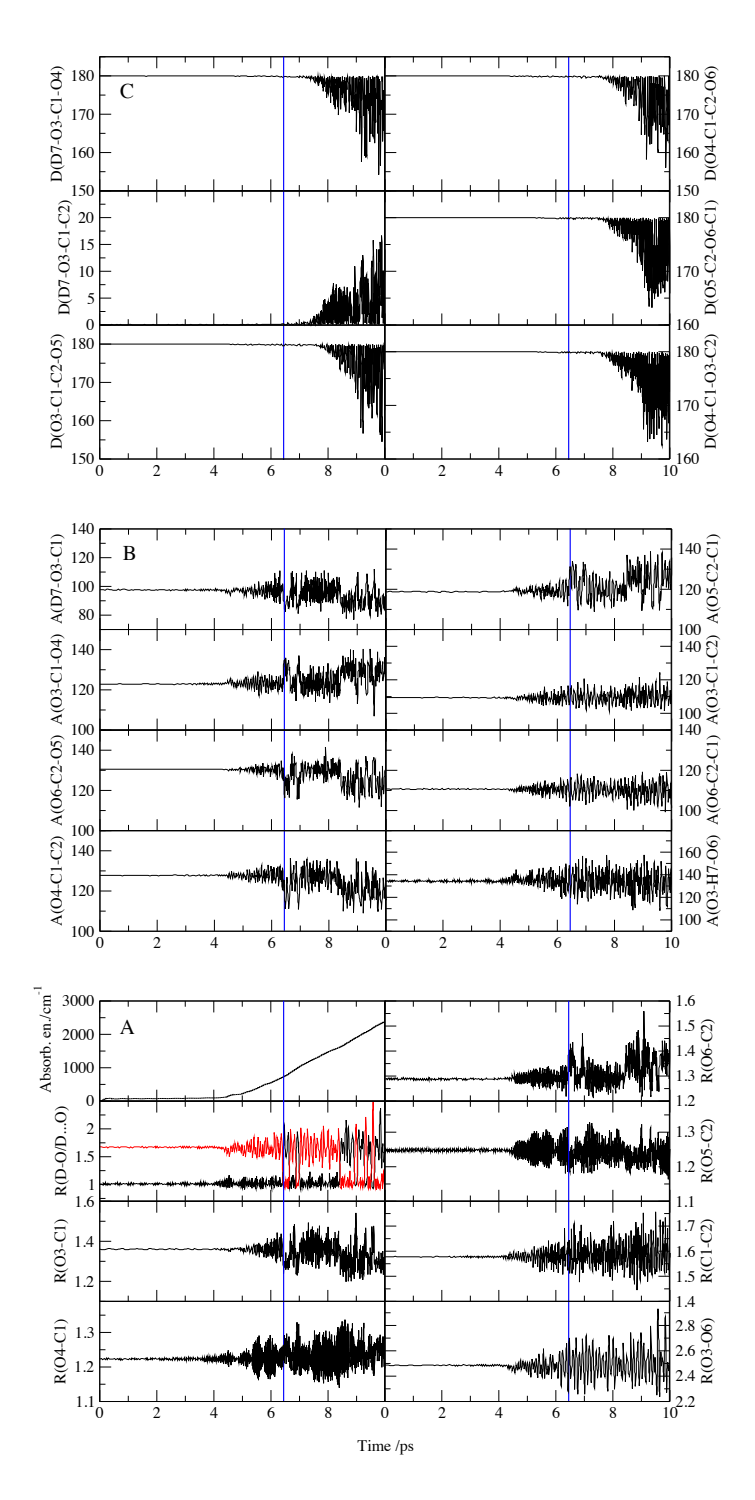


Figure S7. $[C_2O_4D]^-$ DMD trajectory driven at OD-stretching frequency $v_1'=2175$ cm⁻¹. Average absorbed energy is in cm⁻¹, interatomic distances are in Å (bottom panel, A). The D7-O3 distance is shown in black color, while D7...O6 distance in red color. Bond angles (middle panel, B), and dihedral angles (top panel, C) are in degrees. The intensity of the electric field was 130 mV/bohr.

References

- [1] Wolke, C. T.; DeBlase, A. F.; Leavitt, C. M.; McCoy, A. B.; Johnson, M. A. Diffuse Vibrational Signature of a Single Proton Embedded in the Oxalate Scaffold, HO₂CCO₂-. *J. Phys. Chem. A* **2015**, *119*, 13018-13024.
- [2] Humphrey, W.; Dalke, A.; Schulten, K. VMD Visual Molecular Dynamics. *J. Molec. Graphics*, **1996**, *14*, 33-38.